

like mode of the coaxial omniguide. The second issue concerns the ability to transmit information across a broad band of frequencies with the coaxial omniguide. This is determined primarily by the width of the omnidirectional reflectivity range. Another issue is that the multitude of adjustable parameters in the structure of a coaxial omniguide (the index of refraction and thickness of each layer, the thickness of a bilayer, the waveguiding region inner and outer radii, the central rod index of refraction, and so on) allows for great flexibility in tuning the waveguide for optimal desired performance (confinement in the waveguiding region, width of single-mode window, frequency of zero dispersion, group velocity, and so on). A further important issue is that radial confinement of the light is a consequence of omnidirectional reflection and not of total internal reflection. This means that the coaxial omniguide can be used to transmit light around much sharper corners than is possible with the optical fiber. Finally, the radial decay of the electromagnetic field in the coaxial omniguide is much faster than in the case of the optical fiber (with only 10 bilayers, one gets a decrease of electric field intensity of about six orders of magnitude). This means that, for guided light of the same wavelength, the outer diameter of the coaxial omniguide can be much smaller than the diameter of the cladding layer of the optical fiber without leading to cross-talk complications in waveguide bundles. These enabling characteristics of a substantially smaller waveguide bending radius and smaller spacing of adjacent waveguides lead to the possibility of substantial miniaturization of future integrated optical devices and transmission lines.

References and Notes

1. R. A. Waldron, *Theory of Guided Electromagnetic Waves* (Van Nostrand Reinhold, London, 1969).
2. B. E. A. Saleh and M. C. Teich, *Fundamentals of Photonics* (Wiley, New York, 1991).
3. See, for example, S. E. Miller and A. G. Chynoweth, Eds., *Optical Fiber Telecommunications* (Academic Press, New York, 1979).
4. Y. Fink et al., *J. Lightwave Technol.* **17**, 2039 (1999).
5. J. C. Knight et al., *Science* **282**, 1476 (1998).
6. R. F. Cregan et al., *Science* **285**, 1537 (1999).
7. The first attempts at hollow waveguides in the optical regime actually involved metalodielectric materials. See, for example, M. Miyagi et al., *Appl. Phys. Lett.* **43**, 430 (1983), and Y. Matsuura and J. Harrington, *J. Opt. Soc. Am.* **14**, 6 (1997), and references therein.
8. The waveguide also supports transverse magnetic (TM) modes, but they do not appear in the plot because the cutoff frequency for the lowest lying TM mode is larger than $0.30 (2\pi c/a)$.
9. Y. Fink et al., *Science* **282**, 1679 (1998).
10. The idea of radially confining light by means of a dielectric multilayer structure was first investigated by P. Yeh et al. (14). Our work differs in that our waveguide is coaxial, and the multilayer film is chosen so that there exists a frequency range of omnidirectional reflectivity. Both of these properties are important in order to create a TEM-like mode.
11. For example, setting the index of refraction of the coaxial waveguiding region to 1.3 (instead of 1.0), with $n_1 = 4.6$ and $n_2 = 1.8$, the original omnidirectional reflectivity frequency range of 0.17 to 0.25

($2\pi c/a$) in Fig. 2B reduces to a range of 0.18 to 0.23 ($2\pi c/a$), whereas the modal structure shown in Fig. 2C remains essentially unaltered.

12. A. Yariv, *Optical Electronics in Modern Communications* (Oxford Univ. Press, New York, 1997).
13. C. J. Tranter, *Bessel Functions with Some Physical Applications* (Hart, New York, 1969).
14. P. Yeh, A. Yariv, E. Marom, *J. Opt. Soc. Am.* **68**, 1196 (1978).
15. R. D. Meade et al., *Phys. Rev. B* **77**, 8434 (1993); erratum: *Phys. Rev. B* **55**, 15942 (1997).
16. The small discontinuity in $m = 2$ arises from a weak coupling to a resonant mode of the same symmetry localized deep within the core region.
17. N. J. Cronin, *Microwave and Optical Waveguides* (Institute of Physics, Bristol, UK, 1995).
18. For simplicity, we only consider the intrinsic waveguide dispersion in all our calculations. In a real waveguide, we

would also have material dispersion, which can be compensated for in the standard manner by judicious tuning of the waveguide parameters. Indeed, the multitude of available parameters for the coaxial omniguide provides a much greater flexibility to accomplish this than in the case of an optical fiber.

19. We find that the very small group velocity exhibited by the $m = 1$ mode can be driven even to negative values with a proper choice of waveguide parameters.
20. We thank S. Johnson for many helpful discussions. Supported in part by the U.S. Army Research Office under grant DAAG55-97-1-0366, by the Materials Research Science and Engineering Center of NSF under award DMR-9808941, and by the U.S. Department of Energy under grant DE-FG02-99ER45778.

20 March 2000; accepted 25 May 2000

Holes in a Quantum Spin Liquid

Guangyong Xu,¹ G. Aeppli,² M. E. Bisher,² C. Broholm,^{1,3*}
 J. F. DiTusa,⁴ C. D. Frost,⁵ T. Ito,⁶ K. Oka,⁶ R. L. Paul,³
 H. Takagi,⁷ M. M. J. Treacy²

Magnetic neutron scattering provides evidence for nucleation of antiferromagnetic droplets around impurities in a doped nickel oxide-based quantum magnet. The undoped parent compound contains a spin liquid with a cooperative singlet ground state and a gap in the magnetic excitation spectrum. Calcium doping creates excitations below the gap with an incommensurate structure factor. We show that weakly interacting antiferromagnetic droplets with a central phase shift of π and a size controlled by the correlation length of the quantum liquid can account for the data. The experiment provides a quantitative impression of the magnetic polarization cloud associated with holes in a doped transition metal oxide.

Spin density modulations in transition metal oxides are receiving huge attention because of possible connections to high-temperature superconductivity. The modulations appear upon introduction of charge carriers, through chemical substitution, into an insulating and antiferromagnetic parent compound and tend to be static when the carriers are frozen and dynamic when they are mobile. Evidence for such modulations has been largely confined to materials whose magnetism and charge transport are quasi-two-dimensional ($I-4$) and whose parent insulators are ordered antiferromagnets. We provide evidence for analogous phenomena in a quasi-one-dimensional oxide (5), $Y_{2-x}Ca_xBaNiO_5$, for which the parent is a spin liquid by virtue of quantum

fluctuations (6–10) and which has motivated considerable theoretical activity (11–16).

The key features of this orthorhombic material are the chains of NiO_6 octahedra (Fig. 1A). The octahedra are corner-sharing, which results in the dominance of magnetism (8) and electrical conduction (5) by the very simple $\dots O-Ni-O-Ni-O \dots$ backbone. The magnetic degree of freedom at each Ni site is the spin $S = 1$ associated with the $3d^8$ configuration of Ni^{2+} . Each of the $S = 1$ ions is coupled to its neighbors through antiferromagnetic (AFM) superexchange through shared O^{2-} ions. Replacing the off-chain Y^{3+} by Ca^{2+} introduces holes primarily onto apical oxygen atoms in the chains, and while the materials remain insulators, doping substantially increases conductivity at finite temperatures. Thus, $Y_{2-x}Ca_xBaNiO_5$ is a one-dimensional analog of the cuprates, where off- CuO_2 -plane chemical impurities donate holes to the CuO_2 planes.

Magnetic one-dimensionality causes the parent compound Y_2BaNiO_5 to be a spin liquid prevented from ordering antiferromagnetically by quantum fluctuations. The material is not an ordinary paramagnet with heavily damped spin fluctuations, but rather the magnetic analog of superfluid 4He because it has a macroscopically coherent quantum

¹Department of Physics and Astronomy, Johns Hopkins University, Baltimore, MD 21218, USA. ²NEC Research Institute, 4 Independence Way, Princeton, NJ 08540, USA. ³National Institute of Standards and Technology Center for Neutron Research, Gaithersburg, MD 20899, USA. ⁴Department of Physics and Astronomy, Louisiana State University, Baton Rouge, LA 70803, USA. ⁵ISIS Facility, Rutherford Appleton Laboratory, Chilton, Didcot, Oxon OX11 0QX, UK. ⁶Electrotechnical Laboratory, Tsukuba 305, Japan. ⁷Department of Advanced Materials Science, Graduate School of Frontier Sciences, University of Tokyo Hongo, Tokyo 113-8656, Japan.

*To whom correspondence should be addressed. E-mail: broholm@jhu.edu

REPORTS

ground state and lacks static order. Affleck, Kennedy, Lieb, and Tasaki (AKLT) provided a prescription for this state (17, 18). They considered each $S = 1$ degree of freedom as the triplet ground state formed between two ferromagnetically coupled $S = 1/2$ degrees of freedom, in accord with atomic physics, which posits a large and positive Hund's rule coupling between the two $S = 1/2$ holes of Ni^{2+} . To understand the qualitative features of the ground and excited states of the spin-1 chain, they started from the limit of vanishing intraatomic interactions between spin-1/2 holes. Because each site of the spin chain has as many nearest neighbors as $S = 1/2$ degrees of freedom, there exists a macroscopic singlet with the full symmetry of the Hamiltonian wherein all $S = 1/2$ degrees of freedom take

part in nearest neighbor bond singlets (Fig. 2A). Excitations from this "valence bond solid" (VBS) state are triplets formed by broken valence bonds that propagate along the chain. The triplet band is separated from the VBS by an energy of order J corresponding to the energy required to create a triplet at rest. As the ferromagnetic (FM) Hund's rule coupling is taken to much larger values than J , these low-energy states evolve adiabatically into the ground and excited states, respectively, of the $S = 1$ chain. The major change is that for energies below the intraatomic exchange energy, spin-1/2 degrees of freedom can be observed only as edge states, not in the bulk.

The triplet band can be observed experimentally for Y_2BaNiO_5 (Fig. 2A). An image of the magnetic neutron scattering intensity

as a function of wave vector transfer \tilde{q} along the spin chains (in units of the inverse lattice spacing) and energy transfer, $\hbar\omega$, was obtained with time-of-flight neutron spectroscopy at the ISIS Facility in the United Kingdom. Magnetic neutron scattering occurs only when $\hbar\omega$ and \tilde{q} lie on a dispersion relation, thus providing evidence for coherent triplet propagation along spin chains. What distinguishes this excitation from a spin wave is that it propagates in a medium with no static magnetic order. Key features are (i) a 9-meV Haldane gap (19), which corresponds to the threshold energy for triplet creation, (ii) the magnetic excitation bandwidth of 62 meV, which translates into an AFM exchange constant $J = 21$ meV, and (iii) vanishing intensity for $\tilde{q} = n2\pi$, which is evidence for a singlet ground state.

What happens when by Ca doping we add carriers to the quantum spin liquid of Fig. 2A? Our $x = 0.095 \pm 0.005$ sample (Fig. 2B) reveals excitations following a similar dispersion relation as for pure Y_2BaNiO_5 . However, near the former minimum at $\tilde{q} = \pi$, their intensity is substantially reduced and new magnetic scattering appears below the Haldane gap. More detailed data collected near and below the gap (Fig. 3B) show that, near the gap energy, the scattering is peaked at $\tilde{q} = \pi$, but for $\hbar\omega = 3$ to 7 meV, it is most intense along two vertical lines, displaced symmetrically about π . Higher statistics energy-integrated \tilde{q} scans are shown (Fig. 4) that accurately quantify the incommensurate peaks for three single crystals with different levels of doping. Surprisingly, increased doping does not yield a proportional increase in the shift of the peaks from π . Specifically, if we fit the three data sets by the sum of two identical Lorentzians centered at $\pi \pm \delta\tilde{q}$ with half widths at half maximum, $\tilde{\kappa}$, we find that $\delta\tilde{q}$ extrapolates to a finite value in the dilute limit increasing with x as $\delta\tilde{q}(x)/\pi \approx 0.059 \pm 0.002 + (0.25 \pm 0.03)x$ (see inset to Fig. 4B). A similar x dependence is found for $\tilde{\kappa}(x)/\pi \approx 0.047 \pm 0.003 + (0.20 \pm 0.06)x$, with the implication that a single length scale, which is finite in the limit $x \rightarrow 0$, controls both $\tilde{q}(x)$ and $\tilde{\kappa}(x)$.

There are various models that could produce the incommensurate fluctuations we discovered in $\text{Y}_{2-x}\text{Ca}_x\text{BaNiO}_5$. The first proceeds from a charge-ordering hypothesis where the holes order periodically to minimize Coulomb repulsion and the spin system acquires a period commensurate with that of the hole lattice. The magnetic fluctuations are spin waves broadened in \tilde{q} because of disorder in the hole lattice. Such a scenario is commonly supposed for the two-dimensional analog, doped La_2NiO_4 , where key experimental support came from electron (20) and neutron diffraction (21, 22). Thus inspired, we used both techniques to search for hole ordering in $\text{Y}_{2-x}\text{Ca}_x\text{BaNiO}_5$ down to 15 K. The failure of the search makes the charge-

Fig. 1. (A) Chain unit of Y_2BaNiO_5 featuring nickel atoms with octahedral oxygen coordination and Ca^{2+} impurities on Y^{3+} sites. (B) Schematic of $S = 1/2$ degrees of freedom at the edges of the AKLT state. (C) Ferromagnetically coupled chain-end $S = 1/2$ degrees of freedom.

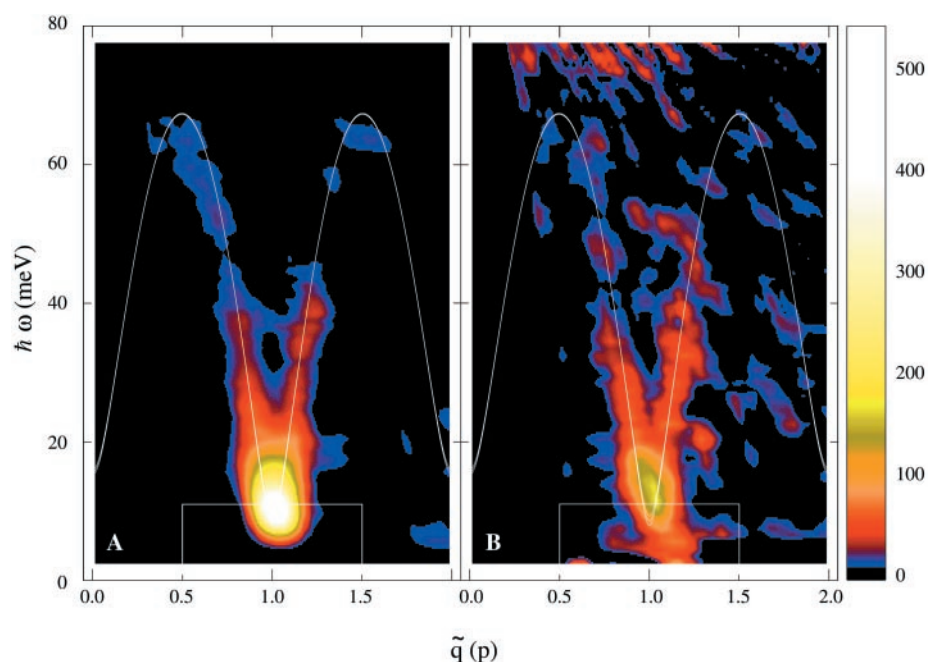
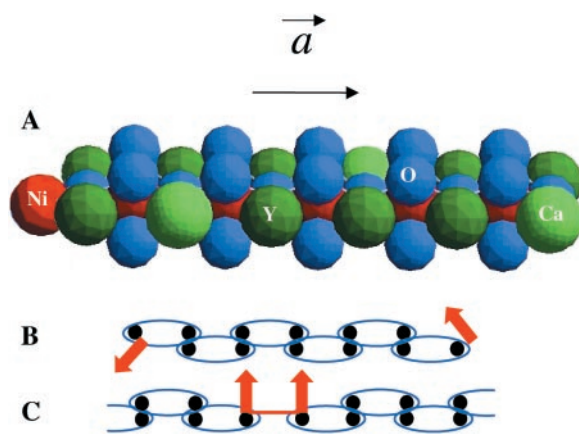


Fig. 2. Overview of magnetic fluctuations in (A) pure and (B) 9.5% doped Y_2BaNiO_5 at $T = 10$ K. The initial neutron beam energy was 90 meV, and the chain axis was perpendicular to the incident beam direction. Boxes indicate regions examined in Fig. 3. The color bar shows values for $\frac{ki}{kf} \frac{d^2\sigma}{d\Omega dE_f}$ in units of mbarn meV^{-1} per Ni.

REPORTS

ordering explanation of our experiments unlikely. Furthermore, in the simplest picture, the hole density has the same period as the spin density squared, so that $\delta\tilde{q}(x)/\pi \approx x$, which is entirely inconsistent with Fig. 4 (dashed line in the inset).

A second possibility is to identify the incommensurate magnetic fluctuations with electron-hole pair excitations from the one-dimensional hole liquid associated with mobile $S = 1/2$ hole propagation through the VBS (11). The wave vectors $\pi \pm \delta\tilde{q}$ would be vectors spanning the Fermi surface, whereas the vertical nature of the incommensurate streaks (Fig. 3) would imply a Fermi velocity exceeding $0.5 \text{ eV}\cdot\text{\AA}$. The problem with this picture is that even if we can ignore that the samples seem not to be proper metals—the resistivities (5) are high at low temperature (T)—the Fermi sea is expected to grow in proportion to x , leading to $\delta\tilde{q}(x) \approx x$, a result again contradicted by Fig. 4.

A last possibility starts from consideration (13) of the magnetic structure factor for a single static hole donated to the NiO chain by the Ca ions. Because it carries a spin, a hole on a superexchange mediating oxygen atom induces an effective FM Ni-Ni interaction (23, 24). The hole-carrying oxygen divides the chain into two semiinfinite segments, for which wave functions can be constructed from a basis set, which is the direct product of wave functions for each segment and for the hole on the intervening oxygen. The ground state wave function for a semiinfinite segment is a doublet rather than the singlet wave function for the unterminated chain. Pictorially (Fig. 1, B and C), the chain ends have unpaired spins because only one of the two AKLT spins, which together represent the $S = 1$ sites, can be paired with an AKLT spin on a neighboring site. The effective FM interaction between semiinfinite chains yields a ground state with inversion symmetry about the oxygen site. The edge states are not localized on Ni^{2+} atoms neighboring the hole but extend into the chain with AFM modulation over a distance of order the Haldane spin correlation length, κ^{-1} . As a result, ground state correlations $\langle S_0 S_j \rangle$ between spins at site 0 and site j , where the FM bond occurs between sites -1 and 0, should take the form $(-1)^j e^{-|j|\kappa}$ for $j \geq 0$ and $(-1)^{j+1} e^{-|j+1|\kappa}$ for $j \leq -1$.

Neutron scattering measures the modulus squared Fourier transform of the spin polarization. For the ground state associated with a single FM bond inserted within an infinite chain, this is

$$S(\tilde{q}) = \left| \frac{(1 + e^\kappa) \cos(\tilde{q}/2)}{\cosh \kappa + \cos \tilde{q}} \right|^2 \quad (1)$$

Equation 1 describes a function with nodes for $\tilde{q} = (2n + 1)\pi$ and pairs of peaks, with half widths and incommensurability of order

κ (see dashed line in Fig. 4A). Thus, the description leading to Eq. 1 does have a chance of accounting for a key feature of our

data. There are, however, three difficulties, the first being that the nodes predicted by Eq. 1 are not seen experimentally. The second

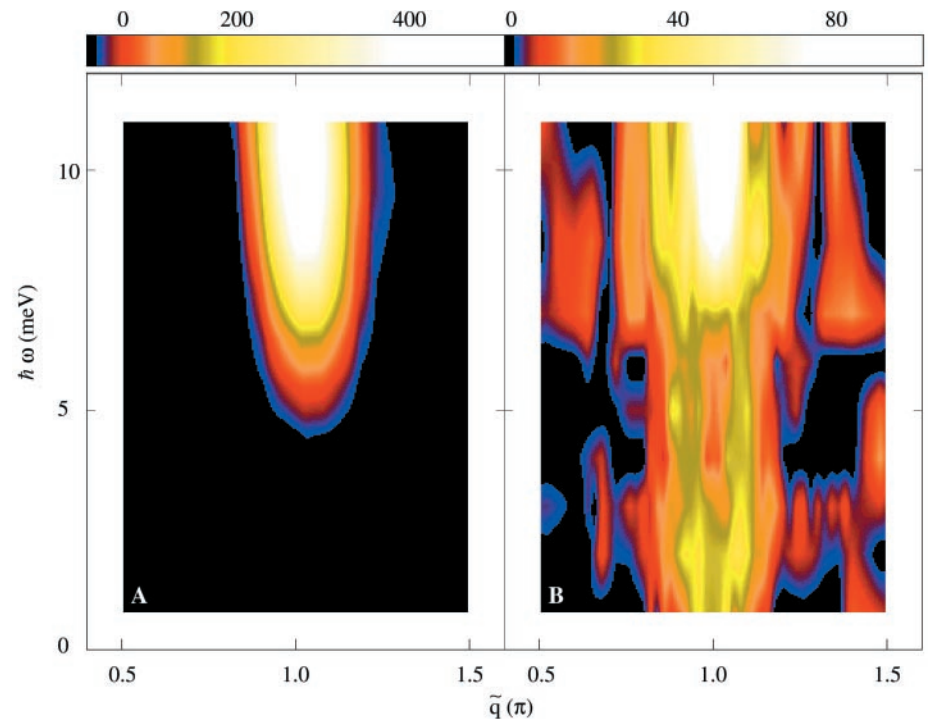


Fig. 3. Low-energy detail of magnetic excitations in (A) pure and (B) 9.5% doped Y_2BaNiO_5 . (A) shows time-of-flight data at $T = 10 \text{ K}$ (MARI spectrometer, ISIS pulsed neutron source), whereas (B) shows data collected at $T = 1.5 \text{ K}$ with triple-axis spectrometers (SPINS and BT2 at NIST steady-state nuclear reactor with final energies of 5 and 14.7 meV, respectively). The color bar shows

values for $\frac{k_i}{k_f} \frac{d^2\sigma}{d\Omega dE_f}$ in units of mbarn meV^{-1} per Ni.

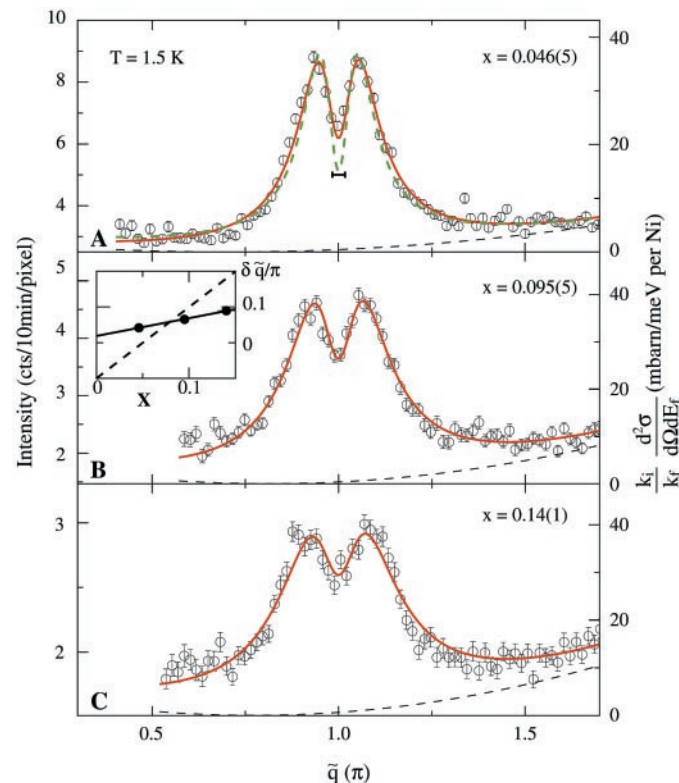


Fig. 4. \tilde{q} scans, collected with SPINS at NIST, through the incommensurate peaks at fixed energy transfer of 4.5 meV for three different hole concentrations: (A) $x = 0.046 \pm 0.005$, (B) $x = 0.095 \pm 0.005$, and (C) $x = 0.14 \pm 0.01$. The energy resolution of the spectrometer was 2 meV full width at half maximum. The dashed green line in (A) shows the single impurity model (Eq. 1) convolved with the instrumental resolution (solid bar). The red lines take into account that neighboring impurities truncate the spin polarization cloud around an impurity bond. The inset in (B) shows half the distance $\delta\tilde{q}(x)/\pi$ between the peaks of two Lorentzians superposed to fit the data.

problem is that we have neglected the spin on the intervening oxygen. The third is that Eq. 1 describes the ground state for a single FM bond, implying that neutron scattering should be elastic, not inelastic as seen experimentally.

The first difficulty has a simple resolution. At finite hole densities, the polarization clouds overlap and the isolated impurity model is inadequate. A crude model, which considers the overlaps, simply truncates the polarization clouds at neighboring impurity sites. Because FM impurity bonds are randomly distributed, the inversion symmetry characterizing isolated impurities is broken, thus allowing intensity at $\tilde{q} = \pi$. Because we know the impurity density, x , from neutron activation analysis, the only parameters in such a description are the extent of the polarization cloud, κ^{-1} , which we adjusted to optimize the fit to our data. As shown by the red lines in Fig. 4, the model provides a good account of the data with $\kappa^{-1} = 8.1 \pm 0.2$, 7.3 ± 0.2 , and 7.2 ± 0.5 for $x = 0.04, 0.095$, and 0.14 respectively. These values are close to the exponential decay length of 6.03 calculated for the AFM spin polarization at the end of an $S = 1$ chain (25).

The modeling described so far does not include the spins of the holes responsible for the effective FM couplings between Ni^{2+} ions. The holes reside in oxygen orbitals of $\text{Y}_{2-x}\text{Ca}_x\text{BaNiO}_5$ (5) but are almost certainly not confined to single, isolated oxygens. We consequently generalized Eq. 1 to take into account the hole spins, with—for the sake of definiteness—the same net amplitude as either of the Ni^{2+} spins next to the FM bond and distributed (with exponential decay) over ℓ lattice sites centered on the FM bond. As long as ℓ exceeds the modest value of 2, comparable to the localization length deduced from transport data (5), the pronounced asymmetry about π that occurs when $\ell = 0$ is relieved sufficiently to produce fits indistinguishable from those in Fig. 4.

How do we account for the inelasticity of the incommensurate signal? One approach is to view the chain as consisting not of the original $S = 1$ degrees of freedom but of the composite spin degrees of freedom induced around holes. The latter interact through overlapping AFM polarization clouds and hole wave functions, to produce effective couplings of random sign because the impurity spacing can be even or odd multiples of the Ni-Ni separation. With weak interchain coupling, the ground state is likely to be a spin glass, as deduced from other experiments (10) on $\text{Y}_{2-x}\text{Ca}_x\text{BaNiO}_5$. The “incommensurate” nature of the excitations continues to follow from the structure factor of the spin part of the hole wave functions.

In summary, we have measured the magnetic fluctuations in single crystals of a doped one-dimensional spin liquid. At energies above the spin gap, the triplet excitations of the parent

compound, Y_2BaNiO_5 , persist with doping. However, below the gap, we find new excitations with a broad spectrum and characteristic wave vectors that are displaced from the zone boundary by an amount of order the inverse correlation length for the parent. The incommensurate fluctuations, encountered here in a doped one-dimensional transition metal oxide, resemble those seen in metallic cuprates. However, one-dimensionality makes them easier to model for Y_2BaNiO_5 , and our analysis reveals that “incommensurate” peaks arise naturally even without hole order because of the characteristic spin density modulation that develops around a defect in the singlet ground state of a quantum spin liquid. This phenomenon accounts for the weak dependence of the incommensurability on doping in the one-dimensional nickelate. Indeed, $\text{Y}_{2-x}\text{Ca}_x\text{BaNiO}_5$ gives us a quantitative impression of the magnetic polarization cloud associated with the holes in a doped transition metal oxide. Our results imply that the spin part of the hole wave function is actually the edge state nucleated by the hole in a quantum spin fluid.

References and Notes

1. S.-W. Cheong *et al.*, *Phys. Rev. Lett.* **67**, 1791 (1991).
2. S. M. Hayden *et al.*, *Phys. Rev. Lett.* **68**, 1061 (1992).
3. H. A. Mook *et al.*, *Nature* **395**, 580 (1998).
4. J. M. Tranquada, B. J. Sternlieb, J. D. Axe, Y. Nakamura, S. Uchida, *Nature* **375**, 561 (1995).
5. J. F. DiTusa *et al.*, *Phys. Rev. Lett.* **73**, 1857 (1994).
6. J. Darriet and L. P. Regnault, *Solid State Commun.* **86**, 409 (1993).

7. J. F. DiTusa *et al.*, *Physica B* **194-196**, 181 (1994).
8. G. Xu *et al.*, *Phys. Rev. B* **54**, R6827 (1996).
9. T. Sakaguchi, K. Kakurai, T. Yokoo, J. Akimitsu, *Phys. Soc. Jpn.* **65**, 3025 (1996).
10. K. Kojima *et al.*, *Phys. Rev. Lett.* **74**, 3471 (1995).
11. E. Dagotto, J. Riera, A. Sandvik, A. Moreo, *Phys. Rev. Lett.* **76**, 1731 (1996).
12. Z.-Y. Lu, Z.-B. Su, L. Yu, *Phys. Rev. Lett.* **74**, 4297 (1995).
13. K. Penc and H. Shiba, *Phys. Rev. B* **52**, R715 (1995).
14. S. Fujimoto and N. Kawakami, *Phys. Rev. B* **52**, 6189 (1995).
15. E. S. Sorensen and I. Affleck, *Phys. Rev. B* **51**, 16115 (1995).
16. R. A. Hyman, K. Yang, R. N. Bhatt, S. M. Girvin, *Phys. Rev. Lett.* **76**, 839 (1996).
17. I. Affleck, T. Kennedy, E. H. Lieb, H. Tasaki, *Phys. Rev. Lett.* **59**, 799 (1987).
18. T. Kennedy, *J. Phys. Condens. Matter* **2**, 5737 (1990).
19. F. D. M. Haldane, *Phys. Lett.* **93A**, 464 (1983).
20. C. H. Chen, S.-W. Cheong, A. S. Cooper, *Phys. Rev. Lett.* **71**, 2461 (1993).
21. J. M. Tranquada, D. J. Buttrey, V. Sachan, J. E. Lorenzo, *Phys. Rev. Lett.* **73**, 1003 (1994).
22. S.-H. Lee and S.-W. Cheong, *Phys. Rev. Lett.* **79**, 2514 (1997).
23. V. J. Emery and G. Reiter, *Phys. Rev. B* **38**, 4547 (1988).
24. A. Aharony *et al.*, *Phys. Rev. Lett.* **60**, 1330 (1988).
25. S. R. White and D. A. Huse, *Phys. Rev. B* **48**, 3844 (1993).

26. We thank T. M. Rice, A. J. Millis, and Q. Huang for useful discussions and A. Krishnan for transmission electron microscopy measurements. Work at Johns Hopkins University was supported by the NSF under DMR-9453362. Work at Louisiana State University was supported by the NSF under DMR-9702690 and the State of Louisiana Board of Regents under LEQSF(RF/1996-99)-RD-A-05. This work used neutron research facilities supported by the National Institute of Standards and Technology (NIST) and the NSF through DMR-9423101.

2 March 2000; accepted 25 May 2000

Subatomic Features on the Silicon (111)-(7×7) Surface Observed by Atomic Force Microscopy

Franz J. Giessibl,* S. Hembacher, H. Bielefeldt, J. Mannhart

The atomic force microscope images surfaces by sensing the forces between a sharp tip and a sample. If the tip-sample interaction is dominated by short-range forces due to the formation of covalent bonds, the image of an individual atom should reflect the angular symmetry of the interaction. Here, we report on a distinct substructure in the images of individual adatoms on silicon (111)-(7×7), two crescents with a spherical envelope. The crescents are interpreted as images of two atomic orbitals of the front atom of the tip. Key for the observation of these subatomic features is a force-detection scheme with superior noise performance and enhanced sensitivity to short-range forces.

In atomic force microscopy (AFM) (1), surfaces are imaged with atomic resolution by bringing a probe into close proximity and

sensing the interaction force while scanning the surface. It has been shown that a dynamic mode of imaging is required for resolving reactive surfaces like Si(111) in an ultrahigh vacuum where chemical bonding between a tip and a sample can occur (2, 3). Frequency-modulation AFM (FM-AFM) (4) enables fast imaging in a vacuum and is now the commonly used imaging technique. In FM-AFM,

Experimentalphysik VI, Center for Electronic Correlations and Magnetism (EKM), Institute of Physics, University of Augsburg, 86135 Augsburg, Germany.

*To whom correspondence should be addressed. E-mail: franz.giessibl@physik.uni-augsburg.de